ISSN 1674-1056
http://cpb.iphy.ac.cn
http://iopscience.iop.org/cpb
中国物理 B
Chinese Physics
中国物理 Chinese Physics B

Conductivity and band alignment of $LaCrO_3/SrTiO_3$ (111) heterostructure

Yan-Peng Hong(洪彦鹏), Xin-Xin Wang(王欣欣), Guo-Liang Qu(曲国良), Cheng-Jian Li(厉承剑), Hong-Xia Xue(薛红霞), Ke-Jian Liu(刘科践), Yong-Chun Li(李永春), Chang-Min Xiong(熊昌民), Rui-Fen Dou(窦瑞芬), Lin He(何林), Jia-Cai Nie(聂家财)
Citation: Chin. Phys. B . 2018, 27(4): 047301. **doi:** 10.1088/1674-1056/27/4/047301

Journal homepage: http://cpb.iphy.ac.cn; http://iopscience.iop.org/cpb

What follows is a list of articles you may be interested in

Electronic states and spin-filter effect in three-dimensional topological insulator Bi_2Se_3 nanoribbons

Genhua Liu(刘根华), Pingguo Xiao(肖平国), Piaorong Xu(徐飘荣), Huiying Zhou(周慧英), Guanghui Zhou(周光辉)
Chin. Phys. B . 2018, 27(1): 017304. **doi:** 10.1088/1674-1056/27/1/017304

Two-dimensional topological insulators with large bulk energy gap

Z Q Yang(杨中强), Jin-Feng Jia(贾金锋), Dong Qian(钱冬)
Chin. Phys. B . 2016, 25(11): 117312. **doi:** 10.1088/1674-1056/25/11/117312

Strain-induced insulator-metal transition in ferroelectric $BaTiO_3$ (001) surface: First-principles study

Lin Yang(杨林), Chang-An Wang(王长安), Cong Liu(刘聪), Ming-Hui Qin(秦明辉), Xu-Bing Lu(陆旭兵), Xing-Sen Gao(高兴森), Min Zeng(曾敏), Jun-Ming Liu(刘俊明)
Chin. Phys. B . 2016, 25(7): 077302. **doi:** 10.1088/1674-1056/25/7/077302

Silicene on substrates: A theoretical perspective

Zhong Hong-Xia, Quhe Ru-Ge, Wang Yang-Yang, Shi Jun-Jie, Lü Jin
Chin. Phys. B . 2015, 24(8): 087308. **doi:** 10.1088/1674-1056/24/8/087308

Stability and electronic structure studies of $LaAlO_3/SrTiO_3$ (110) heterostructures

Du Yan-Ling, Wang Chun-Lei, Li Ji-Chao, Xu Pan-Pan, Zhang Xin-Hua, Liu Jian, Su Wen-Bin, Mei Liang-Mo
Chin. Phys. B . 2014, 23(8): 087302. **doi:** 10.1088/1674-1056/23/8/087302

Conductivity and band alignment of $LaCrO_3/SrTiO_3$ (111) heterostructure*

Yan-Peng Hong(洪彦鹏)†, Xin-Xin Wang(王欣欣)†, Guo-Liang Qu(曲国良)†, Cheng-Jian Li(厉承剑), Hong-Xia Xue(薛红霞), Ke-Jian Liu(刘科践), Yong-Chun Li(李永春), Chang-Min Xiong(熊昌民), Rui-Fen Dou(窦瑞芬), Lin He(何林), and Jia-Cai Nie(聂家财)‡

Department of Physics, Beijing Normal University, Beijing 100875, *China*

(Received 2 November 2017; revised manuscript received 8 January 2018; published online 10 March 2018)

In this work, we investigate the electrical transport property and electronic structure of oxide heterostructure $LaCrO_3/SrTiO_3$ (111). The interface grown under relatively low oxygen partial pressure is found to be metallic with a conducting critical thickness of 11 unit cells of $LaCrO_3$. This criticality is also observed by x-ray photoelectron spectroscopy, in which the Ti^{3+} signal intensity at the spectrum edge of the Ti-$2p_{3/2}$ core level increases rapidly when the critical thickness is reached. The variations of the valence band offset and full width at half maximum of the core-level spectrum with $LaCrO_3$ thickness suggest that the built-in fields exist both in $LaCrO_3$ and in $SrTiO_3$. Two possible origins are proposed: the charge transfer from $LaCrO_3$ and the formation of a quantum well in $SrTiO_3$. Our results shed light on the understanding of the doping mechanism at the polar/non-polar oxide interface. Moreover, due to the interesting lattice and spin structure of LCO in the (111) direction, our work provides a basis for further exploring the novel topological quantum phenomena in this system.

Keywords: oxide heterostructure, $LaCrO_3/SrTiO_3$ (111), x-ray photoelectron spectroscopy, electronic structure

PACS: 73.20.–r, 73.40.–c, 82.80.Pv **DOI:** 10.1088/1674-1056/27/4/047301

1. Introduction

The discovery of a two-dimensional electron gas (2DEG) in $LaAlO_3/SrTiO_3$ (LAO/STO) heterostructure has aroused significant interest in recent years due to a plethora of novel physical phenomena observed at the interface.[1–7] Vast scientific efforts have been made to understand the fundamental physics and apply the LAO/STO heterostructure to the next-generation electronics (see, for example, Refs. [8]–[11]). The discovery of this 2DEG has also facilitated the explorations of other conducting oxide interfaces, such as amorphous LAO/STO,[12,13] $GdTiO_3$/STO,[14] $LaGaO_3$/STO,[15] and amorphous LAO/$La_{1-x}Sr_xMnO_3$/STO.[16]

At another polar/non-polar interface, the $LaCrO_3/SrTiO_3$ (001) (LCO/STO) is reported to be insulating even though a band bending structure is observed in LCO film, which stems from the built-in field in LCO.[17] The analyses of the interfacial structure and composition suggest substantial cation intermixing and partially reducing Ti and Cr ions near the interface, leading to the deviation of interfacial metallicity.[18] In addition, it is found that the $LaAl_{1-x}Cr_xO_3$/STO undergoes a metal-insulator transition when x reaches 0.6, which is speculated to be due to the fact that electrons are trapped in LCO before being transferred to STO due to the multivalence of Cr ions.[19]

Polar-discontinuity also exists in the LCO/STO (111) heterostructure ($(LaO_3)^{3-}$ and Cr^{3+} in LCO while $(SrO_3)^{4-}$ and Ti^{4+} in STO). Whether a 2DEG exists in this system is not only a verification of the validity of the polar catastrophe model, but also important from the viewpoint of material design. In the (111) crystalline orientation, the Cr^{3+} ions in two layers of LCO can form a honeycomb lattice, in which the magnetic moments of adjacent Cr^{3+} ions in the two sublattices of the buckled honeycomb lattice align antiferromagnetically (Fig. 1(a)). Therefore, this system promises to realize both the spinless Haldane model[20,21] and the Kane–Mele model.[22] Theoretical study[23] shows that one unit-cell of another perovskite-type transition-metal oxide grown between LCO (111) honeycomb lattices is possible to realize the quantum spin Hall (QSH) effect or quantum anomalous Hall (QAH) effect, where the spin–orbit coupling is tuned by an electric field. So it is of great scientific significance to study the LCO/STO interface in the (111) direction.

In this work, we fabricate LCO film on STO (111) and investigate the electrical transport property and electronic structure of this heterostructure. It is found that when the oxygen partial pressure (P_{O_2}) used during the deposition of LCO is low, the LCO/STO (111) becomes metallic after 11 unit cells

*Project supported by the National Natural Science Foundation of China (Grant Nos. 11674031, 11474022 11474024, 11422430, and 11374035) and the National Basic Research Program of China (Grant Nos. 2014CB920903, 2013CB921701, and 2013CBA01603).

†Yan-Peng Hong, Xin-Xin Wang, and Guo-Liang Qu made equal contributions to this work.

‡Corresponding author. E-mail: jcnie@bnu.edu.cn

© 2018 Chinese Physical Society and IOP Publishing Ltd

(uc) of the LCO have grown. The band alignment is investigated by x-ray photoelectron spectroscopy (XPS) and the doping mechanism is discussed properly.

2. Experimental procedure

Atomically flat and Ti-terminated STO (111) substrates were prepared by chemical etching for 30 s through using buffered hydrogen fluoride (pH = 5.1) and subsequent annealing in one atmosphere oxygen for 2 h at 910 °C.[24] The LCO film was grown on an STO (111) substrate by the pulsed laser deposition (PLD) technique (KrF laser, 248 nm) from a ceramic target of LCO at P_{O_2} varying from 1.0×10^{-4} Torr (1 Torr = 1.33322×10^2 Pa) to 1.0×10^{-7} Torr. During the film deposition, the laser energy density was 1 J/cm^2 with a repetition rate of 1 Hz and the substrate temperature was kept at 820 °C. After growth, the surface morphology and crystal structure of LCO film was examined by atomic force microscopy (AFM) and x-ray diffraction (XRD), respectively.

Sheet resistance was measured by the four-point method. For the Hall effect measurement, the sample was mechanically-patterned in hall-bar geometry with 600 μm in length and 250 μm in width. The contacts were made of 25-micron diameter Al wires through ultrasonic bonding. The transport properties were measured at temperatures ranging from 300 K to 13 K and magnetic field up to 1 T.

Without any surface treatment, the as-grown samples are sent *ex situ* to the XPS chamber with a base pressure of about 1×10^{-10} torr. The x-ray source is monochromatic 150-W Al Kα radiation with an energy resolution of 0.45 eV. The XPS spectra were collected in the direction normal to the surface at room temperature. During measurement, an electron gun was used to help us avoid the charging effect due to the insulating nature of some samples. In addition, the binding energy obtained was corrected by using the C-1s (284.6 eV). For all samples, a Shirley background has been subtracted from the raw data.

3. Results and discussion

3.1. Morphology and structure

The LCO is an insulator with a pseudo-cubic lattice parameter of 3.885 Å, excellently matching to STO (3.905 Å). A typical surface morphology of an 18-uc (∼ 4.5 nm) LCO film grown on STO (111) under a P_{O_2} of 5×10^{-6} Torr is shown in Fig. 1(b). It shows an atomically flat surface that inherits from the STO substrate, indicating the layer-by-layer growth model is achieved. In Fig. 1(b), the height of the step edge is measured to be 0.25 nm (not shown here), which is equal to the lattice constant of LCO in the (111) direction. The crystal structure of LCO film is examined by XRD, which is shown in Figs. 1(c) and 1(d). The films are epitaxial with the (111) single phase character with the lattice constant of the LCO film expanding to a larger value (∼ 3.954 Å) due to the low P_{O_2} [25,26] as can be seen clearly in Fig. 1(d). In our work, the thickness of the thin film is examined by x-ray reflection (XRR) (inset of Fig. 1(d)).

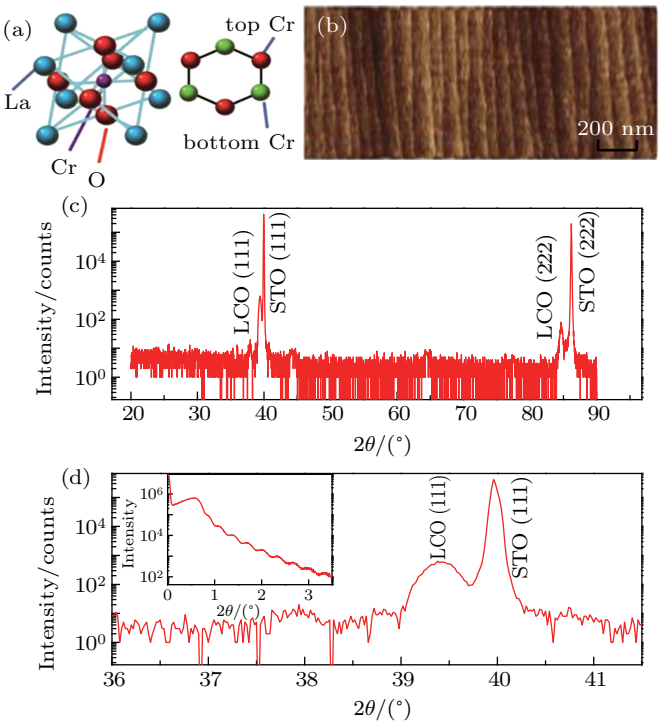


Fig. 1. (color online) (a) Left: lattice structure of the perovskite LCO with atom species labeled. Right: buckled honeycomb lattice formed by two adjacent layers of Cr atoms viewed from the (111) crystal direction. Spheres in green and red indicate two kinds of spins with opposite directions. (b) Surface morphology of an 18-uc LCO film grown under oxygen partial pressure of 5×10^{-6} Torr on Ti-terminated STO (111) substrate. (c) The x-ray diffraction of a 10-nm LCO on STO (111). (d) Zoom-in drawing around the (111) peak. Inset shows a typical XRR of the LCO/STO (111).

3.2. Electrical transport property

Figure 2(a) shows the room-temperature sheet resistance for LCO/STO (111) with 5-nm LCO (> 11 uc) grown under various P_{O_2} values. The heterostructures grown under P_{O_2} higher than 5×10^{-6} Torr are highly insulating. Although the sample grown under 5×10^{-6} Torr shows measurable sheet resistance at room temperature, it is semiconducting (inset in Fig. 2(c)). For samples grown in P_{O_2} lower than 1×10^{-6} Torr, the critical thickness of conductivity is determined to be 11 uc as shown in Fig. 2(b). Figure 2(c) shows the temperature dependence of sheet resistance for LCO (11 uc)/STO grown under 5×10^{-7} Torr. It is metallic when cooled down to 13 K. The Hall resistance is linear with the magnetic field in the measured magnetic field range (Fig. 2(e)). From the Hall measurements, the sheet carrier density at the interface decreases from 3.8×10^{13} cm^{-2} at room temperature to 1.8×10^{13} cm^{-2} at 13 K, and the mobility increases from 4 cm^2/V·s to 100 cm^2/V·s (Fig. 2(d)), similar to the typical value reported for LAO/STO.

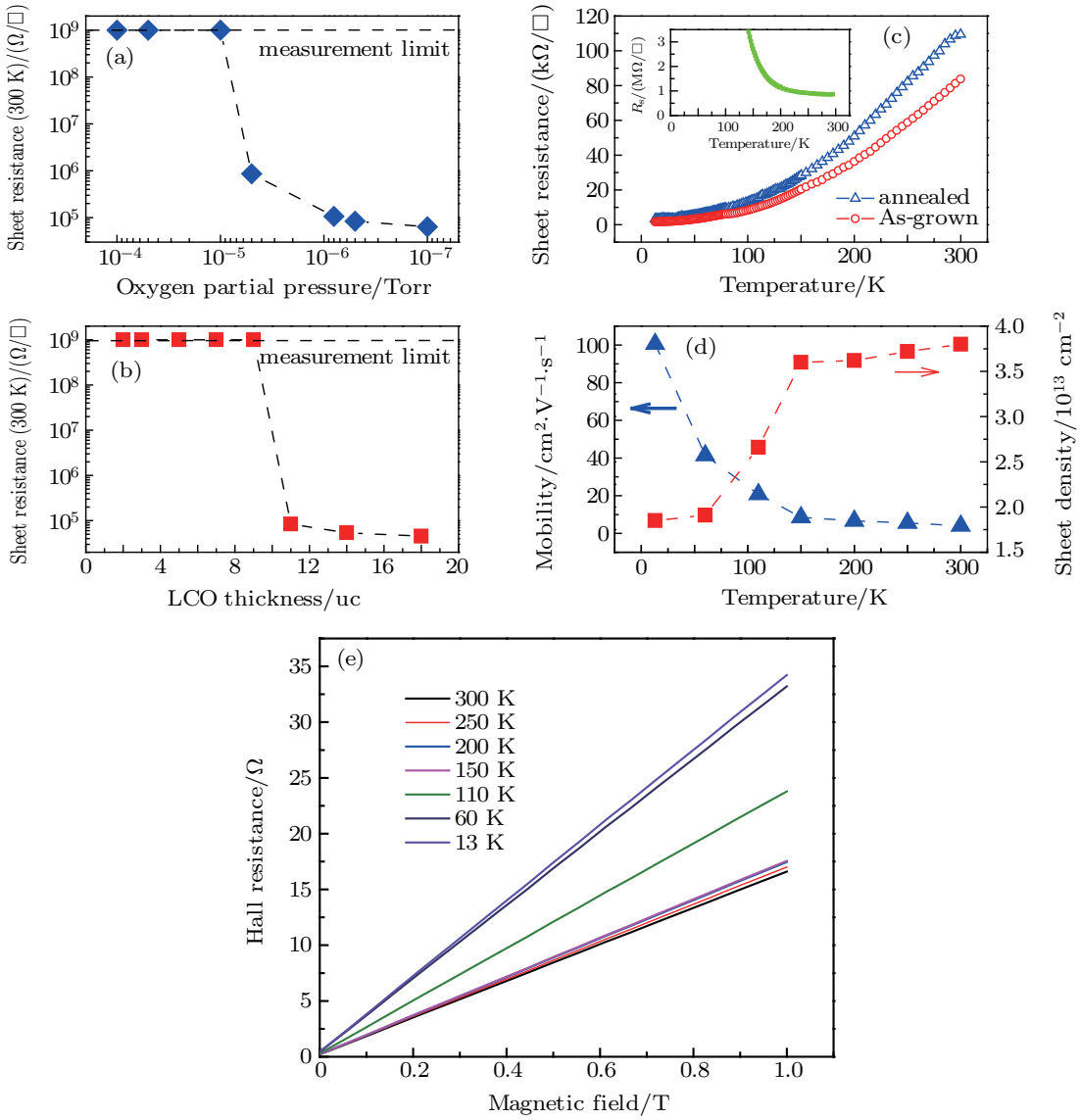


Fig. 2. (color online) (a) Room-temperature sheet resistance for LCO/STO (111) with 5 nm (> 11 uc) LCO as a function of P_{O_2} adopted during growth. (b) LCO thickness dependence of sheet resistance measured at room temperature of LCO/STO (111) grown under 5. $\times 10^{-7}$ Torr. (c) Temperature dependence of sheet resistance in a temperature range from 300 K to 13 K for LCO/STO (111) with 11-uc LCO grown under 5×10^{-7} Torr. Red circles represent the values measured after growth while blue triangles refer to the values measured after annealing. Inset shows the temperature dependence of sheet resistance for LCO (11 uc)/STO (111) grown under 5×10^{-6} Torr. (d) Temperature dependences of mobility (blue triangle) and sheet carrier density (red square) from Hall measurement for LCO (11 uc)/STO (111) grown under 5×10^{-7} Torr. (e) Plots of Hall resistance versus magnetic field at various temperatures for LCO (11 uc)/STO (111) grown under 5×10^{-7} Torr). The dashed lines are guides to the eye.

Due to the bombardment of high-energy plasma plume and surface redox reaction,[12] oxygen vacancies may be formed in STO substrate when LCO is deposited at high temperature and low P_{O_2} These vacancies can dope STO with electrons thus making it metallic. However, after annealing in one atmosphere of oxygen at 420 °C for 6 h the metallic samples are still conducting as shown in Fig. 2(c) for an LCO/STO sample with 11-uc LCO. Besides, a homoepitaxial 30-unit-cells-thick STO film grown on an STO substrate at P_{O_2} of 5×10^{-7} Torr is insulating. These observations exclude the decisive factor of oxygen vacancy in interfacial conductivity and point to the existence of other doping mechanisms at this interface.

3.3. Ti-2p$_{3/2}$ core level

As previously stated, for LCO/STO (111), the onset of metallicity comes when the thickness of LCO reaches 11 uc. This criticality is also observed in the XPS Ti-2p$_{3/2}$ core-level spectrum (Fig. 3). For all LCO thicknesses measured, the spectrum is mainly composed of the Ti^{4+} peak (peak 1 in Fig. 3). However, when the LCO thickness is 11 uc, a peak (green areas in Fig. 3(f)) appears at about 2-eV lower in energy than the Ti^{4+} main peak and becomes more and more obvious when LCO gets thicker (Figs. 3(g) and 3(h)). This low energy

peak is an unambiguous signature of the Ti^{3+} signal, which is an indication of electron doping of STO.[27,28] The relative content of Ti^{3+} is calculated as the ratio between the area under the Ti^{3+} peak and the area under the entire fitting curve. Results together with the peaks-fitting parameters are listed in Table 1. It is shown that while the Ti^{3+} relative content is very small for LCO thinner than 11 uc, it increases abruptly to 5.02% at 11-uc LCO and further increases to 7.38% and 8.55% for 14 uc and 18-uc LCO, respectively. A similar magnitude of the Ti^{3+} relative content is also reported in the literature for the conducting LAO/STO interface.[18,29] Note that except for the two peaks mentioned above, there is one additional peak that is about 0.9 eV lower than the Ti^{4+} peak (peak 2 in Fig. 3). The signals of 2-uc and 3-uc samples are invisible or small, but they become evident when the thickness of LCO is 5 uc, well below the critical thickness of 11 uc, and nearly keeps constant upon increasing the LCO thickness. This peak is also seen in LAO/STO[29] but its origin is unspecific so far.

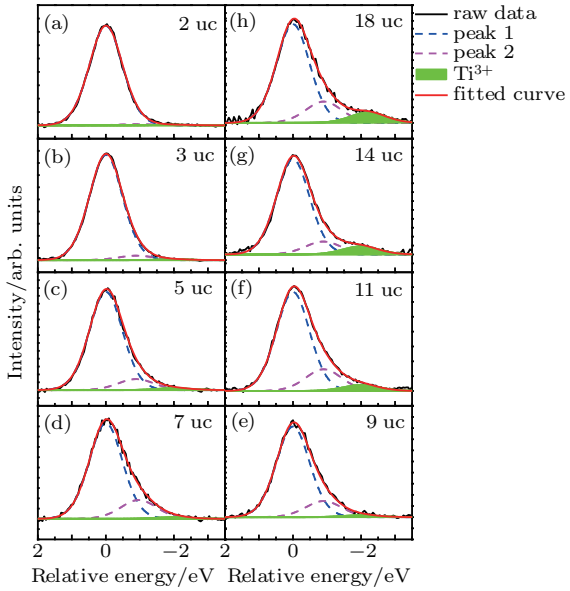


Fig. 3. (color online) Peak decompositions of the Ti-$2p_{3/2}$ spectra in LCO/STO (111) with various LCO thickness values. The spectra are shifted to the Ti^{4+} main peak (dashed blue). The green area highlights the Ti^{3+} peak and the red solid line presents the fitted curve. Before fitting, a Shirley background is subtracted from the raw data.

Table 1. Parameters used for fitting the Ti-$2p_{3/2}$ core-level spectrum of LCO/STO (111) in Fig. 3. The FWHMs for the Ti^{4+} main peak (peak 1 in Fig. 3), peak 2 and Ti^{3+} peak are listed. ΔBE1 is the energy separation between Ti^{4+} and peak 2. ΔBE2 is the energy separation between Ti^{4+} and Ti^{3+}. The percentage of corresponding peak is the ratio between the area under the peak and that under the entire fitting curve with uncertainty estimated at ±5% of the base value.

LCO thickness/uc	Peak 1 (Ti^{4+}) FWHM	Peak 2 FWHM	Ti^{3+} FWHM	ΔBE1 /eV	ΔBE2 /eV	Relative of peak 2/%	Relative of Ti^{3+}/%
2	1.15	1.25	1.25	0.9	2	1.19	0.62
3	1.15	1.25	1.25	0.9	2	4.35	0.64
5	1.15	1.25	1.25	0.89	1.99	10.68	1.78
7	1.15	1.25	1.25	0.95	1.98	17.33	1.51
9	1.15	1.25	1.25	0.9	2	15.88	1.83
11	1.15	1.25	1.25	0.9	2	18.27	5.02
14	1.15	1.25	1.25	0.9	2	11.85	7.38
18	1.15	1.25	1.25	0.9	2.2	17.43	8.55

3.4. Valence band offset and built-in field

To further understand the mechanism of the conductivity in LCO/STO (111), we investigate the electronic structure of the heterostructure by XPS. The valence band offset (VBO), ΔE_V, can be calculated from the following formula:[30]

$$\Delta E_V = \left(E_{La4d_{5/2}} - E_{VBM1}\right)_{LCO} - \left(E_{Sr3d_{5/2}} - E_{VBM2}\right)_{STO} + \Delta E_{HJ},$$

where the $\left(E_{La4d_{5/2}} - E_{VBM1}\right)_{LCO}$ ($\left(E_{Sr3d_{5/2}} - E_{VBM2}\right)_{STO}$) is the binding energy difference between core level of La-$4d_{5/2}$ (Sr-$3d_{5/2}$) and valence band maximum (VBM) in bulk LCO (STO). In our work, $E_{La4d_{5/2}}$ is the binding energy of the La-$4d_{5/2}$ core level measured in LCO/STO (111) with thick LCO film (18 uc) and the E_{VBM1} is the binding energy of VBM of LCO in the same sample, which is determined by extrapolating the leading edge of the VB spectrum to the energy axis in order to account for the instrumental broadening (Figs. 4(a) and 4(b)). The VBM of LCO (E_{VBM1}) is measured to be 0.52 ± 0.05 eV (Fig. 4(a)) and $\left(E_{La4d_{5/2}} - E_{VBM1}\right)_{LCO}$ is 101.92 ± 0.05 eV. To deduce the VBM of STO (111) (E_{VBM2}), an Nb-doped (0.7 wt%) STO (111) substrate is used after the same chemical etching and annealing procedure as that of undoped STO. By adopting the same linear method used for E_{VBM1}, the E_{VBM2} and the $\left(E_{Sr3d_{5/2}} - E_{VBM2}\right)_{STO}$ are measured to be 2.8 ± 0.05 eV (Fig. 4(b)) and 130.65 ± 0.05 eV, respectively. Here the value of the later is a little larger than that of the (001) direction, which is 130.54 eV from Chambers.[31] $\Delta E_{HJ} = \left(E_{Sr3d_{5/2}} - E_{La4d_{5/2}}\right)_{HS}$ is the difference in binding energy between Sr-$3d_{5/2}$ and La-$4d_{5/2}$ core level measured at the LCO/STO (111) heterostructure and it is an interfacial property. The value of ΔE_{HJ} first increases from 27.82 ± 0.05 eV to 28.31 ± 0.05 eV when the thickness of LCO increases from 2 uc to 11 uc and then reaches to a plateau of 28.23 ± 0.05 eV at 18 uc.

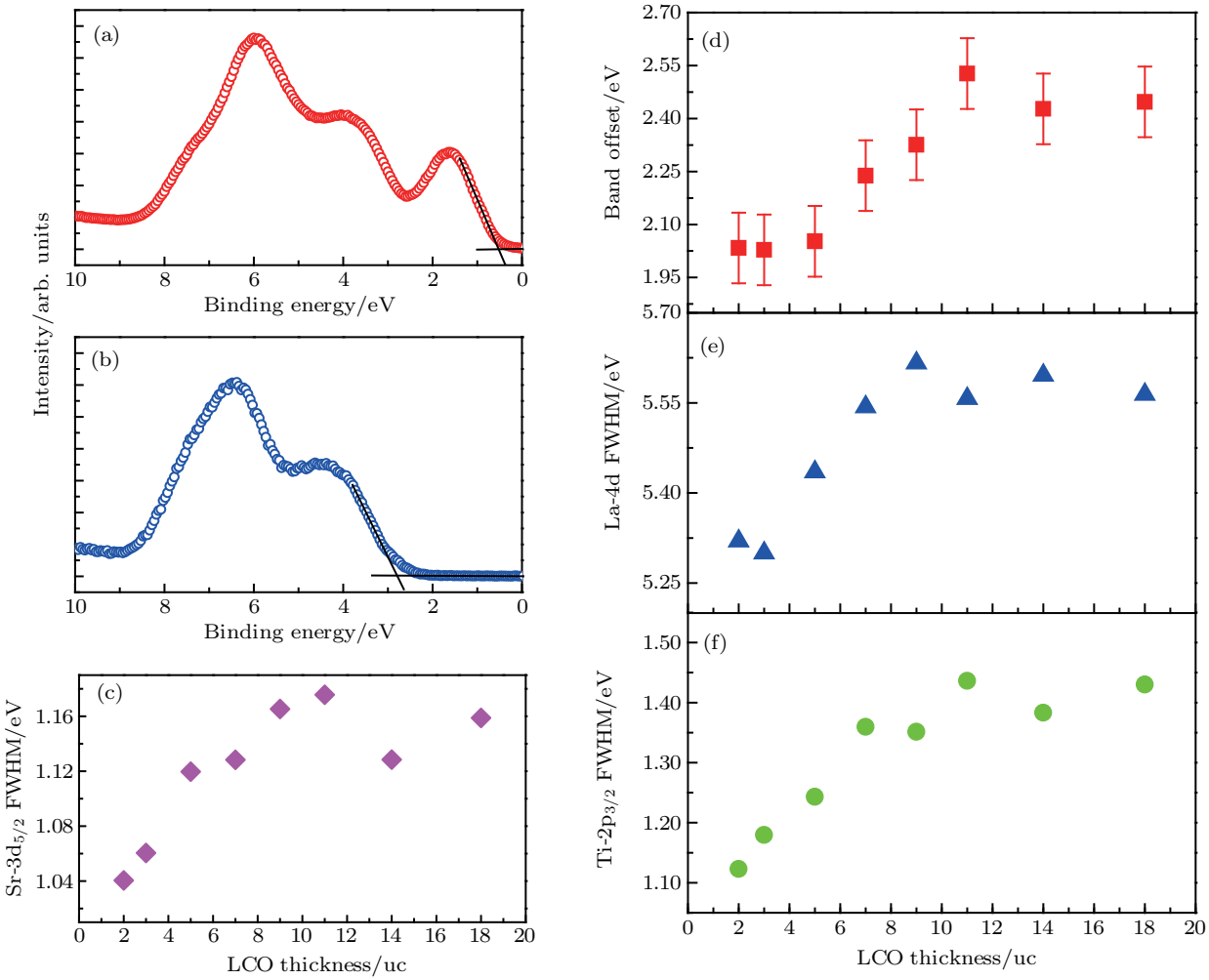


Fig. 4. (color online) (a) VB spectra measured for LCO (18 uc)/STO (111) and (b)STO (111) substrate. (c) LCO-thickness dependence of FWHM of Sr-$3d_{5/2}$ core-level spectrum, (d) VBO, (e) FWHMs of La-4d core-level spectrum, and (f) FWHMs of Ti-$2p_{3/2}$ core-level spectrum.

Using the above formula, the VBO of LCO/STO (111) heterostructure can be calculated. The result is shown in Fig. 4(d) for various thickness values of LCO. It can be seen that the VBO increases with the thickness of LCO increasing, and goes to a plateau after 11 uc, where it peaks at 2.45 ± 0.05 eV. The increase of VBO with LCO thickness increasing indicates the existence of a built-in field in LCO, which is also evidenced by the increasing of the full width at half maximum (FWHM) of La-4d core-level peak with LCO thickness increasing (Fig. 4(e)). The increase of FWHM with LCO thickness increasing results from peak-broadening of the La-4d core-level spectrum due to the built-in field in LCO, which will lead to the increasing of electron energy in LCO. Our results on the tendency and magnitude of VBO and FWHM are comparable to the results of Chambers.[17]

3.5. Discussion

At a polar-discontinuous interface, a potential energy divergence problem usually arises and is deemed to trigger the interfacial metallicity at LAO/STO (001) according to the polarization catastrophe model, in which it is believed that the electrons at VBM of LAO transfer to the bottom of the conduction band of STO at the critical thickness (4 uc).[9] Indeed, the observed increase of VBO and FWHM with LCO thickness increasing as well as the existence of a built-in field in LCO is a reflection of energy divergence. However, the observed magnitude of VBO at a critical thickness of 11 uc LCO (2.45 ± 0.05 eV) is less than the energy gap of STO (3.2 eV) (Fig. 4(d)). Small VBO is also reported in LAO/STO[32] and it is now recognized in the literature that this discrepancy can be reasonably explained when the surface states in LAO, such as in-gap states induced by oxygen vacancies, are considered.[33–36] In the present study, due to the low P_{O_2} used for growing a conducting LCO/STO (111) interface, it is possible that electrons donated by oxygen vacancies in the film reside in the in-gap states of LCO that is higher in energy than LCO's VBM. Due to the increase of potential with LCO thickness increasing, electrons in these in-gap states can be transferred to STO at a critical thickness of 11 uc, at which the energy of in-gap states in LCO equals the energy of STO's conduction band (Fig. 5(a)).

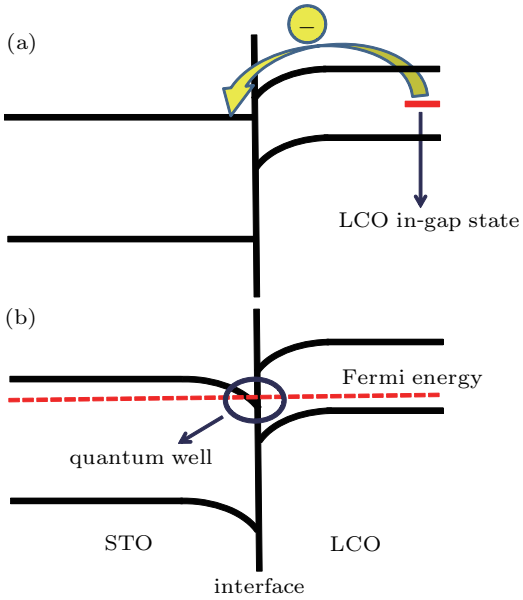


Fig. 5. (color online) (a) Schematic illustration of charge-transfer mechanism and (b) quantum well formation used to explain the origin of interfacial metallicity (see text).

Another explanation of the interfacial metallicity can be made after inspecting the electron structure on the STO side. Figure 4(f) displays the FWHM of Ti-$2p_{3/2}$ core-level spectrum as a function of LCO thickness. The FWHM of the Ti-$2p_{3/2}$ core level has the same tendency as VBO and FWHM of La-$4d_{5/2}$ (Figs. 4(d) and 4(e)). The variation of the FWHM of Ti-$2p_{3/2}$ we have observed is large compared with Chambers's results,[17] in which the FWHMs of Ti-$2p_{3/2}$ and Sr-$3d_{5/2}$ core level change to a less extent than the FWHMs of Cr-3p and La-4d. In Ref. [17], the small variation in FWHM of Ti-$2p_{3/2}$ is explained as the consequence of out-diffusion of Ti ions into LCO film, leading to the presence of $Ti^{3+\delta}$. Although the variation in FWHM of the Sr-$3d_{5/2}$ core level is also small in our work (Fig. 4(c)), the relatively large change in the FWHM of the Ti-$2p_{3/2}$ core level should be mainly ascribed to the built-in field in the STO substrate, not just to the Ti out-diffusion during growth. From the band-diagram viewpoint, this built-in field in STO indicates a band bending downward and a notched structure forming in STO near the interface (Fig. 5(b)), which is widely observed at the conducting LAO/STO interface.[37,38] This notched structure in STO can lead to the formation of a quantum well at an interface at the critical thickness of 11 uc, at which the STO conduction band passes through the Fermi level (Fig. 5(b)).

4. Conclusions

In this work, we fabricate a high-quality LCO/STO (111) heterostructure by the PLD method and investigate the electrical transport property and electronic structure. The LCO/STO (111) heterostructure grown in P_{O_2} lower than 1×10^{-6} Torr is metallic when the thickness of LCO is no less than 11 uc. From the observation of XPS, the Ti^{3+} signal in the Ti-$2p_{3/2}$ core-level spectrum shows an abrupt increase at 11 uc. The magnitude of VBO, and the FWHMs of La-$4d_{5/2}$ and Ti-$2p_{3/2}$ all increase with LCO thickness increasing, indicating bands bending in LCO film and STO substrate. While the oxygen vacancy forming in the substrate during growth can be ruled out as a major source of interfacial conductivity, the interfacial metallicity can be explained as a consequence of the charge-transfer process in which electrons in LCO in-gap state transfer to STO due to potential energy divergence. Alternatively, the metallicity may be related to the quantum well forming at STO. Our work provides an insight into the origin of 2DEG found at LAO/STO and other polar/non-polar interface. Moreover, due to the interesting lattice and spin structure of LCO in the (111) direction, our work provides a basis for further exploring the novel topological quantum phenomena in this system.

References

[1] Ohtomo A and Hwang H Y 2004 *Nature* **427** 423
[2] Reyren N, Thiel S, Caviglia A D, Kourkoutis L F, Hammerl G, Richter C, Schneider C W, Kopp T, Ruetschi A S, Jaccard D, Gabay M, Muller D A, Triscone J M and Mannhart J 2007 *Science* **317** 1196
[3] Brinkman A, Huijben M, Van Zalk M, Huijben J, Zeitler U, Maan J C, van der Wiel W G, Rijnders G, Blank D H and Hilgenkamp H 2007 *Nat. Mater.* **6** 493
[4] Caviglia A D, Gariglio S, Reyren N, Jaccard D, Schneider T, Gabay M, Thiel S, Hammerl G, Mannhart J and Triscone J M 2008 *Nature* **456** 624
[5] Bert J A, Kalisky B, Bell C, Kim M, Hikita Y, Hwang H Y and Moler K A 2011 *Nat. Phys.* **7** 767
[6] Dikin D, Mehta M, Bark C, Folkman C, Eom C and Chandrasekhar V 2011 *Phys. Rev. Lett.* **107** 056802
[7] Li L, Richter C, Mannhart J and Ashoori R C 2011 *Nat. Phys.* **7** 762
[8] Nakagawa N, Hwang H Y and Muller D A 2006 *Nat. Mater.* **5** 204
[9] Hwang H Y, Iwasa Y, Kawasaki M, Keimer B, Nagaosa N and Tokura Y 2012 *Nat. Mater.* **11** 103
[10] Cen C, Thiel S, Mannhart J and Levy J 2009 *Science* **323** 1026
[11] Woltmann C, Harada T, Boschker H, Srot V, van Aken P A, Klauk H and Mannhart J 2015 *Phys. Rev. Appl.* **4** 064003
[12] Chen Y Z, Pryds N, Kleibeuker J E, Koster G, Sun J R, Stamate E, Shen B G, Rijnders G and Rijnders S 2011 *Nano Lett.* **11** 3774
[13] Herranz G, Sánchez F, Dix N, Scigaj M and Fontcuberta J 2012 *Sci. Rep.* **2** 758
[14] Moetakef P, Cain T A, Ouellette D G, Zhang J Y, Klenov D O, Janotti A, Van de Walle C G, Rajan S, Allen S J and Stemmer S 2011 *Appl. Phys. Lett.* **99** 232116
[15] Perna P, Maccariello D, Radovic M, Scotti di Uccio U, Pallecchi I, Codda M, Marré D, Cantoni C, Gazquez J, Varela M, Pennycook S J and Miletto Granozio F 2010 *Appl. Phys. Lett.* **97** 152111
[16] Chen Y Z, Trier F, Wijnands T, *et al.* 2015 *Nat. Mater.* **14** 801
[17] Chambers S A, Qiao L, Droubay T C, Kaspar T C, Arey B W and Sushko P V 2011 *Phys. Rev. Lett.* **107** 206802
[18] Colby R, Qiao L, Zhang K H L, Shutthanandan V, Ciston J, Kabius B and Chambers S A 2013 *Phys. Rev. B* **88** 155325
[19] Kumar P, Pal P, Shukla A K, Pulikkotil J J and Dogra A 2015 *Phys. Rev. B* **91** 115127
[20] Haldane F D M 1988 *Phys. Rev. Lett.* **61** 2015
[21] Xiao D, Zhu W G, Ran Y, Nagaosa N and Okamoto S 2011 *Nat. Commun.* **2** 596
[22] Kane C J and Mele E J 2005 *Phys. Rev. Lett.* **95** 226801
[23] Liang Q F, Wu L H and Hu X 2013 *New J. Phys.* **15** 063031
[24] Koster G, Kropman B L, Rijnders G J H M, Blank D H A and Rogalla H 1998 *Appl. Phys. Lett.* **73** 2920
[25] Yun K Y, Noda M and Okuyama M 2003 *Appl. Phys. Lett.* **83** 3981

[26] Hong R J, Qi H J, Huang J B, He H B, Fan Z X and Shao J D 2005 *Thin Solid Films* **473** 58
[27] Takizawa M, Tsuda S, Susaki T, Hwang H Y and Fujimori A 2011 *Phys. Rev. B* **84** 245124
[28] Drera G, Salvinelli G, Brinkman A, Huijben M, Koster G, Hilgenkamp H, Rijnders G, Visentin D and Sangaletti L 2013 *Phys. Rev. B* **87** 075435
[29] Koitzsch A, Ocker J, Knupfer M, Dekker M C, Dörr K, Büchner B and Hoffmann P 2011 *Phys. Rev. B* **84** 245121
[30] Qiao L, Droubay T C, Kaspar T C, Sushko P V and Chambers S A 2011 *Surf. Sci.* **605** 1381
[31] Chambers S A, Englehard H M, Shutthanandan V, Zhu Z, Droubay T C, Feng T, Lee H D, Gustafsson T, Garfunkel E, Shah A, Zuo J M and Ramasse Q M 2010 *Surf. Sci. Rep.* **65** 317
[32] Segal Y, J. Ngai J H, Reiner J W, Walker F J and Ahn C H 2009 *Phys. Rev. B* **80** 241107
[33] Bristowe N C, Littlewood P B and Artacho E 2011 *Phys. Rev. B* **83** 205405
[34] Slooten E, Zhong Z, Molegraaf H J A, Eerkes P D, de Jong S, Massee F, van Heumen E, Kruize M K, Wenderich S, Kleibeuker J E, Gorgoi M, Hilgenkamp H, Brinkman A, Huijben M, Rijnders G, Blank D H A, Koster G, Kelly P J and Golden M S 2013 *Phys. Rev. B* **87** 085128
[35] Zhou J, Asmara T C, Yang M, Sawatzky G A, Feng Y P and Rusydi A 2015 *Phys. Rev. B* **92** 125423
[36] Yu L P and Zunger A 2014 *Nat. Commun.* **5** 5118
[37] Yoshimatsu K, Yasuhara R, Kumigashira H and Oshima M 2008 *Phys. Rev. Lett.* **101** 026802
[38] Han Y L, Fang Y W, Yang Z Z, Li C J, He L, Shen S C, Luo Z Z, Qu G L, Xiong C M, Dou R F, Wei X, Gu L, Duan C G and Nie J C 2015 *Phys. Rev. B* **92** 115304